Structural and Optical Properties of GO- doped (TiO2:MoS2) Films Prepared by Pulsed Laser Deposition

Zeina S. Mahdi
Physics Dept., College of Science, Univ. of Baghdad, Baghdad, Iraq

Ghuson H. Mohammed
Physics Dept., College of Science, Univ. of Baghdad, Baghdad, Iraq

Abstract

With focused Nd:YAG laser beam at 400mJ with a second radiation at 1064nm (pulse width 9ns) repetition frequency (6Hz), for 200 laser pulses incident on target surface, pulsed laser deposition (PLD) had been utilized for preparing (TiO2:MoS2)1-x(GO)x films at RT onto glass substrates at various concentration of GO (0.06, 0.12, 0.18, 0.24 and 0.30). The goal of the investigation is to determine how GO content affects the films' morphological, structural, electrical, and optical properties. Various methods, including Atomic Force Microscope (AFM), X-ray diffraction (XRD), UV-Vis spectroscopy, and the Hall Effect, have been used for characterizing thin films. According to the findings, films have been polycrystalline and displayed small peaks in the case when doped with GO material. The deposited TiO2:MoS2's XRD peaks have been improved as the GO concentration rose. In the case when GO is added to a structure, the average diameter and roughness are measured using AFM, with GO ratio 0.30 yielding the highest value. Optical transmission has been examined by using a UV-vis spectrophotometer. It was discovered that as GO content in films increased, so did transmittance.

1. Introduction

Various categories of materials are especially interesting for many applications, like the microelectronics, nano-scale, energy, computer science, safety engineering, transportation, technology, military, electrical appliances, and optoelectronic devices, among others, according to development and research on transition elements. [1]. The Transparent Conducting Oxide Semiconductors (TCOs) class of semiconductor materials includes titanium dioxide (TiO2). It has low conductivity, absorbs ultraviolet (UV) light, and is highly transparent in visible spectrum [2]. White pigment, corrosion protection, gas sensors, and optical coatings are just a few examples of the industrial uses for (TiO2), which is categorized as group (II-VI). TiO2 is a chemically inert substance. [3] Solar cells [4], environmental purification [5], high electrical resistance and high dielectric constant [6, 7], and the ability to be used as coatings on glass to create self-cleaning glass [8] are a few examples. Two sulfur atoms and one molybdenum atom make up the inorganic compound known as molybdenum disulfide (MoS2), which belongs to the transition metal dichalcogenides (TMD) series. Dichalcogenides are created chemically when a chalcogen (an element from group 16 of periodic table), such sulfur (S), is combined with a transition metal such as molybdenum [9].

Many researchers were interested in this compound because of its unique chemical, physical, and electrical properties, which

included its huge band gap (1.8eV) that changes from indirect to direct gap in thin structures. Thus, it might be able to downscale electronic devices [10, 11]. MoS2 is used in a variety of fields, such as optical sensors and sensing. [12, 13]. Oxygen, carbon, and hydrogen quantities vary in graphitic oxide, sometimes called graphene oxide (GO). Strong oxidizers and acids are used to dissolve any excess metals in graphite to create it. In the case when C:O ratio is between 2.1 and 2.9, maximally oxidized bulk is a yellow solid with a layer structure resembling graphite, yet with irregular and broader spacing. [14] [15]. Physical and chemical properties of graphene include electrical conductivity [19], mechanical strength [18], transparency [17], and thermal conductivity [16]. Desorption/ionization [20], electronics [21], and water desalination [22] are a few uses for graphene. The synthesis and characterization regarding optically transparent (TiO2:MoS2) films at various GO NPs that were deposited on glass substrates are discussed in the current research. The (TiO2:MoS2): GO thin films' morphological, structural, electrical, and optical characteristics are assessed by XRD, AFM, hall effect, and UV-vis. spectroscopy.

2. Experimental

(2-1) Sample Preparations

TiO20.98:MoS20.02 (purity of 99.99%) was combined with GO NPs at various concentrations (0.06, 0.12, 0.18, 0.24, and 0.3), and the mixture was after that ground together for 10 mins in a gate mortar. In order to create pellets with 0.2 cm thickness and 1 cm diameter, it is then compressed collectively through a hydraulic press at a pressure of 5 tons and for 10 minutes. After being sintered for an hour at 700 ° C, the pellets have been cooled to the temperature of the room.

(2-2) Thin Film Deposition

With the use of the prepared palettes, (TiO2:MoS2)1-xGOx thin films have been applied at RT to a glass substrate measuring 2.5 x 7.5 cm before being ultrasonically washed for 15 mins. With the use of a PLD with a 1064nm wavelength and an energy of 400mJ Nd: YAG laser, thin films were created. On the target surface with a 45 ° angle, replicate frequency (6Hz) is present for 200 laser pulses. The deposits were created at (1×10-1) mbar of chamber pressure. The distance between the substrate and the target was 10 cm. The interference approach was used to calculate the film thickness as being about 200±5 nm.

(2-3) Measurements

Through the use of the Cu-Kα (λ = 0.154nm) over 2θ scan range of 10o-80o, structural characteristics of (TiO2:MoS2)1-x(GO)x thin films were investigated by XRD by using a Panalytical X'Pert Pro X-ray diffractometer system. AFM has been utilized in order to examine film's surface morphological characteristics. With the use of a UV-vis-NIR spectrophotometer (Metertech SP-8001), the optical characteristics of thin films were investigated. It was the (190-1100 nm) wavelength range. The ECOPIA HALL EFFECT MEASUREMENT SYSTEM (HMS-3000 VER 3.52) has been utilized in order to study electrical characteristics of thin films.

3. Results and discussion

(3-1) XRD Results.

The XRD regarding doped TiO2:MoS2 thin films with various GO contents are depicted in Figure 1. According to (ASTM) cards, the thin films' structure revealed a polycrystalline tetragonal structure with a hexagonal phase for MoS2, a rutile phase for TiO2, and a

hexagonal phase as well for GO. Figure 1 shows that the peaks at 2 equal to 27.45, 36.07, 41.19, and 54.32 correspond to reflection from the (110), (100), (101), and (001) planes of hexagonal MoS2, rotileTiO2, and hexagonal GO, respectively, at concentrations of (0.06, 0.12, and 0.18), respectively, from GO. The peaks that appeared at 2θ, which is equal to 27.43, 36.11, 41.23, and 54.34, respectively, are reflections from (110), (100), (101), and (001) at concentrations of 0.24 GO. The peaks appeared at 2θ equal to 27.45, 36.07, 41.26, 54.34, and 63.95 are reflections from (110), (100), (101), (001), and (310) at concentrations of 0.30, respectively. The Debye-Scherer's equation was utilized to determine the crystal's size (Cs) [23]

$$C_s = \frac{0.9\,\lambda}{\beta \cos\theta} \quad (1)$$

where λ represent the X-rays' wavelength, $\boldsymbol{\beta}$ represent FWHM and θ represent angle of diffraction, and for calculating strain(ε), we apply the next equation [24]

$$\varepsilon = \frac{\beta_{hkl}}{4\,tan\theta} \quad (2)$$

Dislocation density (δ) which could be represented through dislocation lines' length to crystal size, could be specified with the use of the next relation[25]

$$\delta = \frac{1}{C_s^2} \quad (3)$$

Average size of the crystallite Cs, inter-planar distance, micro strain ε dislocation and number of the planes have been estimated as well based on Debye Scherer equations, and results have been presented in Table1 for the planes in the pattern of diffraction of and doped the (TiO2:MoS2)1-x(GO)x thin films.

Fig. 1: XRD of (TiO2:MoS2) doped with various GO NPs' contents

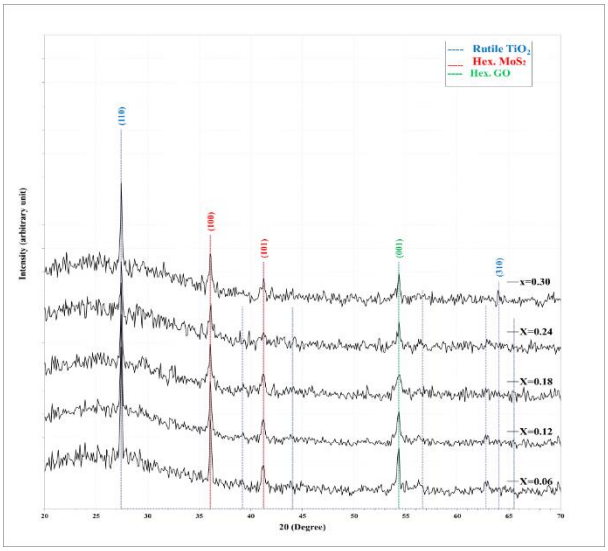

Table 1: Shows inter-planer distance (dhkl,) FWHM, and crystal size for (TiO2:MoS2) thin films doped with various GO NPs' contents

Sample	2θ (Deg.)	FWHM (Deg.)	d_{hkl} (Å)	d_{hkl} Std. (Å)	C.S (nm)	hkl	Phase	δx10^{15} (line/m^2)	$\boldsymbol{\varepsilon}$
X=0.06	27.4589	0.2107	3.2456	3.2483	38.8	(110)	RutileTiO_2	0.66	0.00089
	36.0767	0.2529	2.4876	2.4871	33.1	(100)	Hex.MoS2	0.92	0.00105
	41.1968	0.3582	2.1895	2.1871	23.7	(101)	Hex. MoS2	1.78	0.00146
	54.3236	0.2529	1.6874	1.6874	35.3	(001)	Hex. GO	0.80	0.00098
X=0.12	27.4589	0.1896	3.2456	3.2483	43.1	(110)	RutileTiO_2	0.54	0.00080
	36.0767	0.2529	2.4876	2.4871	33.1	(100)	Hex. MoS2	0.92	0.00105
	41.1968	0.3371	2.1895	2.1871	25.2	(101)	Hex. MoS2	1.58	0.00138
	54.3447	0.3372	1.6868	1.6874	26.5	(001)	Hex. GO	1.42	0.00131
X=0.18	27.4589	0.1686	3.2456	3.2483	48.5	(110)	RutileTiO_2	0.42	0.00071
	36.0767	0.2528	2.4876	2.4871	33.1	(100)	Hex. MoS2	0.91	0.00105
	41.1968	0.3161	2.1895	2.1871	26.9	(101)	Hex. MoS2	1.39	0.00129
	54.3658	0.4214	1.6862	1.6874	21.2	(001)	Hex. GO	2.22	0.00164

X=0.24	27.4378	0.2107	3.2480	3.2483	38.8	(110)	RutileTiO_2	0.66	0.00089
	36.1188	0.2739	2.4848	2.4871	30.5	(100)	Hex. MoS2	1.07	0.00114
	41.2389	0.3582	2.1874	2.1871	23.7	(101)	Hex. MoS2	1.78	0.00146
	54.3447	0.3372	1.6868	1.6874	26.5	(001)	Hex. GO	1.42	0.00131
X=0.30	27.4589	0.2107	3.2456	3.2483	38.8	(110)	RutileTiO_2	0.66	0.00089
	36.0767	0.2528	2.4876	2.4871	33.1	(100)	Hex. MoS2	0.91	0.00105
	41.2600	0.3371	2.1863	2.1871	25.2	(101)	Hex. MoS2	1.58	0.00138
	54.3447	0.2739	1.6868	1.6874	32.6	(001)	Hex. GO	0.94	0.00106
	63.9528	0.2318	1.4546	1.4527	40.4	(310)	RutileTiO_2	0.61	0.00086

(3-2) Atomic force microscopic

As can be seen in figure (2) and Table (2), a 3D image of (TiO2:MoS2) thin films doped with various concentrations of GO particles enables us to learn about surface morphology of films that have been formed on glass substrates at the RT as well as a mean roughness, grain size, and RMS from AFM images. It was seen from the images that the films' surfaces had a specific amount of roughness, and that the roughness of the film increased with concentration. According to this finding, surface roughness increases when larger grains form and are concentrated more. Additionally, it has been found that when concentration increases, so does the average particle size. Depending on the film concentration, the average grain size values ranged from (212.7 -391.1) nm. This might be because larger clusters are produced by the coalescence of at least two grains. Additionally, RMS of the surface increases by the addition of GO, indicating the development of grains with regular shapes on surface. According to a prior work by [26], high RMS implies that the surface area of GO/TiO2:MoS2 thin film was high, which will result in more light absorption.

Fig.2: 3-D AFM images of (TiO2:MoS2) thin films that have been doped with various GO contents that have been prepared at room temperature.

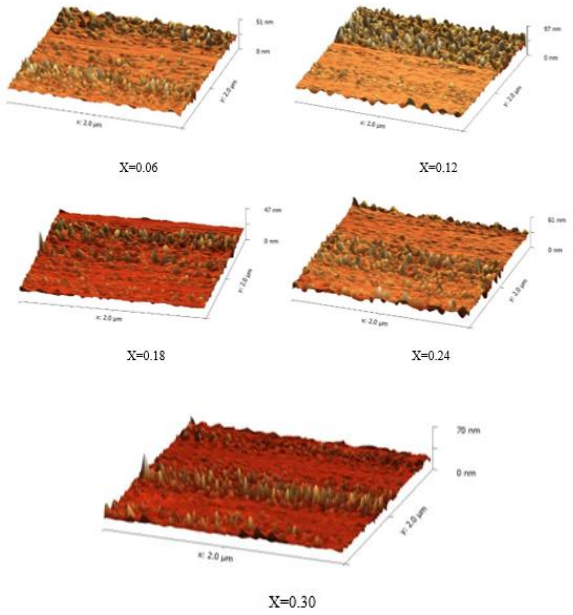

Table2: Average roughness, RMS, and grain size for (TiO2:MoS2) thin films at various concentration of GO at the temperature of the room.

Samples	Avg. grain size (nm)	Avg. roughness (nm)	RMS (nm)
X=0.06	212.7	8.31	2.60
X=0.12	243.9	8.58	3.30
X=0.18	314.1	9.23	3.65
X=0.24	387.9	9.65	3.68
X=0.30	391.1	10.78	4.32

(3-3) The optical properties

The transmission, extinction coefficient, absorption coefficient, dielectric constant, refractive index, and optical energy gap of doped (TiO2:MoS2) thin film with various content of GO (0.06, 0.12, 0.18, 0.24, and 0.30) wt. have been measured as well as recorded in wave-length ranges of (400nm-1100nm. Figure3 depicts the transmission spectrum fluctuation with wave-length for films that have been made of (TiO2:Mos2): GO at various GO concentrations. Because the transmittance value is inversely correlated with GO concentration, it falls as GO content rises in (TiO2:MoS2) films. This could be brought on by an increase in heavy atoms that would result in increasing the absorption. However, the decrease in the transmission could result from the peak moving to lower energies as a result of the formation of levels close to the energy band gap. This conclusion is consistent with Khorsand's findings [27]. Also, with increasing GO, the decrease in transmittance (increase in absorption) may be due to the addition of GO particles to the TiO2:MoS2.

Fig.3: Transmittance spectra of (TiO2:MoS2) thin films doped with different GO contents.

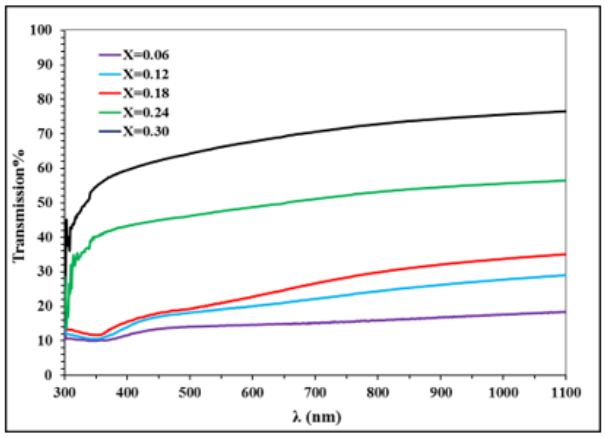

Fig.4: Absorption coefficient of (TiO2:MoS2) thin films doped with various GO contents.

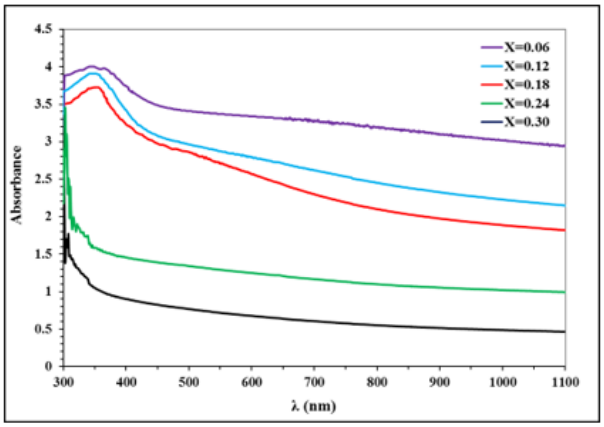

The coefficient of absorption could be found according to the equation [28,29]

$$\alpha = 2.303\ A/t \quad (4)$$

where A represents absorbance and t represents sample's thickness.

Optical energy gap value could be estimated through the next equation [30]

$$\alpha h\nu = B(h\nu - Eg)r \quad (5)$$

Eg stands for optical band gap, r represents exponent that indicates type of the optical transitions that can occur in the material, hv represent incident photon's energy, and B represent a constant that inversely relates to the amourphousity. Absorption in UV region (one hole and one electron) increases significantly as a result of band-to-band absorption that takes place in the case where an electron is elevated from valence to conduction bands and produces a new pair of charge carriers. The increased GO concentration (x) makes the material opaquer (more absorbance), which causes Eg to decrease. The rise in localized states' density in conduction band or valence band, ready to take electrons and form optical energy gap tails that are attempting to close the energy

gap, is how we explain this phenomenon. A smaller band gap might be attributed to many-body interaction effects that happen between free carriers and ionized impurities or charge carriers [31].

Fig.5: Plot of (α hυ)2 as a function of hυ for (TiO2:MoS2) thin films doped with different contents of GO.

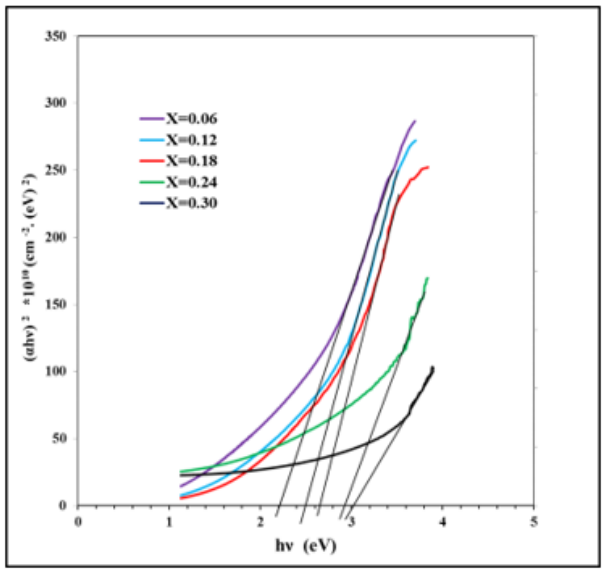

Figure 6 shows how the extinction coefficient (k) varies with wave-length in (300 - 1100nm) range for samples prepared at room temperature. Table 3 demonstrates that the value of K increases with the amount of doping, and the next relation could be used to determine its value [32].

$$k=\frac{\alpha\lambda}{4\Pi} \quad (6)$$

Fig.6: The extinction coefficient (k) for (TiO2:MoS2) thin films doped with various contents of GO

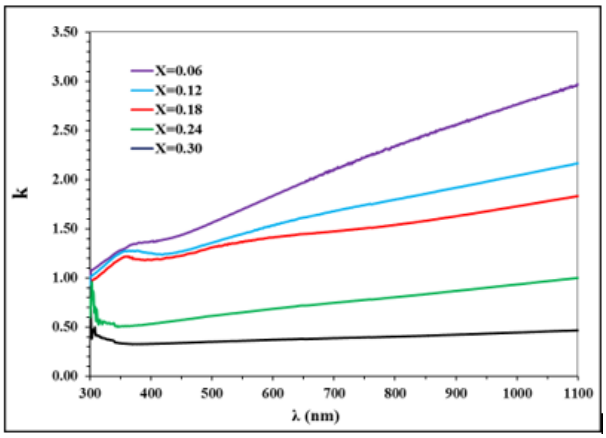

The refractive index fluctuation of doped (TiO2:MoS2) with varying (GO) content in (400nm-1100nm) wavelength range has been depicted in Figure7 and Table3. It is evident that when the doping level rises, the refractive index decreases.

Fig.7: Refractive index for (TiO2:MoS2) thin films that are doped with various GO contents

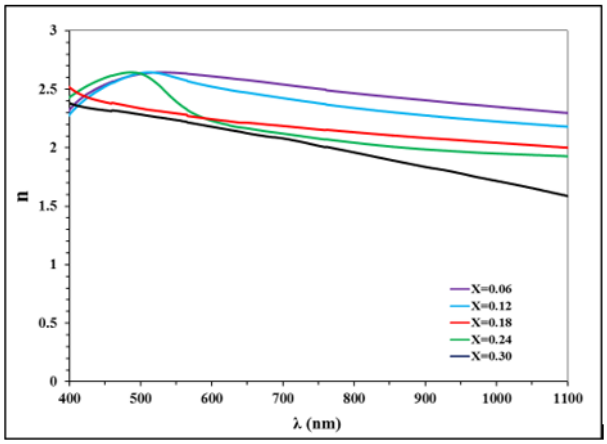

Relation describing complex optical refractive index of the film[33]

$$n^*=n - iK \quad (7)$$

In which n* represent complex refractive index (n) and (k) represent real and imaginary parts of the complex refractive index, and

simple refractive index could be found based on the equation [34]

$$n=\frac{1+R}{1-R}+\sqrt{\frac{4R}{(1-R)2}}-K2 \quad (8)$$

the imaginary and real parts of dielectric constant are functions of wavelength in doped (TiO2:MoS2) thin films with varying GO concentrations in a wavelength range of (450-1100nm) at the temperature of the room, as can be seen from Figs. 8 and 9. The real part depends on the value of (n2) primarily because of how small the value of (k2) is in comparison to it, whereas the imaginary part depends on the value of (k), with indicated in Table (3), it has been discovered that their values increased by increasing amount of doping, and that their values decreased when the amount of wavelength increased. They may be estimated by using the eqs. [35]

$$\varepsilon_r = n2\text{-}k2 \quad (9)$$
$$\varepsilon_i = 2\ nk \quad (10)$$

Fig.8: The real part for (TiO2:MoS2) thin films doped with various GO contents.

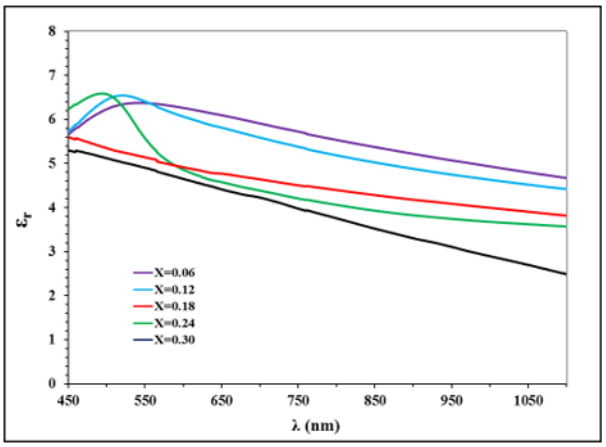

Fig.9: The imaginary part for TiO2:MoS2) thin films doped with various GO contents

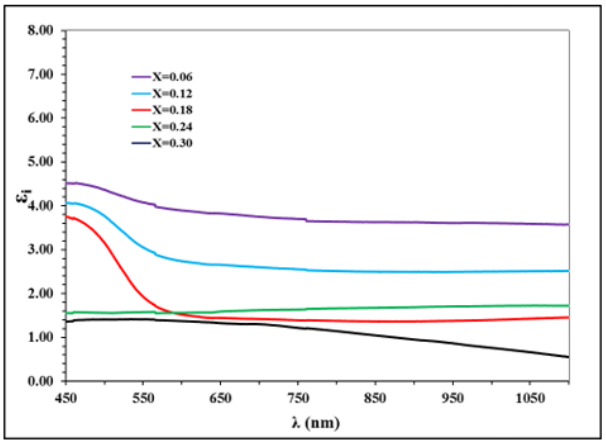

Table (3): transition, absorption coefficient and optical constant for (TiO2:MoS2) doped (GO) in proportions at room temperature.

Sample	T%	α (cm^{-1})	K	n	ε_r	ε_i	Eg (eV)
X=0.06	66.18	82563	0.362	2..630	6.575	1.405	3.00
X=0.12	47.58	148544	0.650	2.386	6.449	1.562	2.90
X=0.18	20.94	312774	1.370	2.284	6.235	3.157	2.70
X=0.24	19.16	330475	1.447	2.263	5.349	3.768	2.50
X=0.30	14.37	387948	1.699	2.250	5.118	4.364	2.20

3-5 Hall Effect

Investigations were done on Hall Effect measurements of varying GO contents in both and undoped doped (TiO2:MoS2) thin films. GO doped (TiO2:MoS2) thin films' electrical properties, including carrier concentration (n), conductivity (σ), Hall mobility (H), and others, were assessed at room temperature

with the use of the 4-point probe (Van Der Pauw) resistivity approach and Hall measurement by applying a 0.25T magnetic field. Using equation (1.15), the Hall coefficient RH was calculated.

RH=1/n.e for p-type (11)

RH coefficient's positive sign suggests that all samples are p-type. (in other words, the conduction is dominated by holes). For (TiO2:MoS2) thin films with various GO doping concentrations, the values of carrier concentration (nH) and Hall mobility (H) were obtained with the use of equations (11) and the next equation, respectively:

$\mu H = \sigma/ne$

It is evident that when the GO content rises, the carrier concentration nH rises and Hall mobility H decreases. The additional charge carriers brought on by doping are what caused the increase in charge carrier density. While the inverse relationship between H and nH is what causes the decreasing mobility.

Table (4) Hall Effect measurements for (TiO2:MoS2) thin film with various concentration GO content.

Sample X	$\sigma *10^{-5}$ $(\Omega.cm)^{-1}$	$\rho* 10^{4}$ $(\Omega.cm)$	R_H $(cm^{-3}.C^{-1})$	n_H*10^{12} (cm^{-3})	μ $(cm^2/V.S)$	type
0.06	2.086	4.795	1.048E+6	3.290	40.33	P
0.12	2.822	3.543	8.612E+7	5.529	24.30	P
0.18	2.091	4.783	1.129E+6	5.956	23.60	P
0.24	2.052	4.873	8.458E+5	7.249	21.86	P
0.30	2.125	4.705	1.897E+6	7.380	17.36	P

Conclusion

This study has looked into how the GO content affects morphological, structural, electrical, and optical characteristics of the thin films made of (TiO2: MoS2). The presence of weak, very small peaks in XRD pattern reveals that the films are polycrystaline in nature. The ratio of 0.30 % GO has been found as the optimal one amongst among the other ratios (highest roughness and largest crystalline size), and it may be utilized in order to create various products, such as optoelectronic devices, according to AFM and XRD performance. With regard to all samples, the refractive index and dielectric (real part) decrease, whereas the extinction coefficient and dielectric constant (imaginary part) increase with an increase in the doping ratio. For all of the samples, the coefficient of absorption increases as the doping ratio increases and has a (> 104cm -1) value. According to our research, TiO2: MoS2 doped with different GO concentrations is the best device for solar cell applications.

Reference

[1] K. Gesheva et al., “Optical, structural and electrochromic properties of sputter-deposited W-Mo oxide thin films,” J. Phys. Conf. Ser., vol. 764, no. 1, 2016, doi: 10.1088/1742-6596/764/1/012010.

[2] M. Walczak, E.L. Papadopoulou, M. Sanz, A. Manousaki, J.F. Marco, and M. Castillejo." Structural and morphological characterization of TiO2 nanostructured films grown bynanosecond pulsed laser

deposition " Applied Surface Science. 31,(2010) p.250.

[3] B. R. Sankapal, M.C. Lux-Steiner, A. Ennaoui: Synthesis and characterization of anatase-TiO2 thin films. Applied Surface Science. v.239, n.2, p.165-170, (2005).

[4] B. O'Regan, M. Gratzel: A low-cost, high-efficiency solar cell based on dyesensitized colloidal TiO2 films. Nature. v.353, n., p.737-740, (1991).

[5] S. Ikezawa, H. Homyara, T. Kubota, R. Suzuki, S. Koh, F. Mutuga, T. Yoshioka, A.Nishiwaki, Y. Ninomiya, M. Takahashi, K. Baba, K. Kida, T. Hara, T. Famakinwa: Applications of TiO2 film for environmental purification deposited by controlled electron beam-excited plasma. Thin Solid Films. v.386, n.2, p.173-176, (2001).

[6] H. Cheng, J. Ma, Z. Zhao, L. Qi: Hydrothermal preparation of uniform nanosize rutile and anatase particles. Chemistry of Materials. v.7, n., p.663-671, (1995).

[7] M. Gopal, W. J. M Chan, L. C. de Jonghe: Room temperature synthesis of crystalline metal oxides. Journal of Materials Science. v.32, n.; p.6001-6008, (1997).

[8] E. M. Paula e Silva: A tecnologia, suas estratégias, suas trajetórias. Ciência e Cultura. v.60, n.spel, p.13-21, (2008).

[9] He, Z.; Que, W. Molybdenum Disulfide Nanomaterials: Structures, Properties, Synthesis and Recent Progress on Hydrogen Evolution Reaction. Appl. Mater. Today 2016, 3, 23–56.

[10] Novoselov, K. Beyond the Wonder Material. Phys. World 2009, 22, 27–30.

[11] Moutaouakil, A.E.; Kang, H.-C.; Handa, H.; Fukidome, H.; Suemitsu, T.; Sano, E.; Suemitsu, M.; Otsuji, T. Room Temperature Logic Inverter on Epitaxial Graphene-on-Silicon Device. Jpn. J. Appl. Phys. 2011, 50, 070113.

[12] Weng, X.; Neethirajan, S. Immunosensor Based on Antibody-Functionalized MoS2 for Rapid Detection of Avian Coronavirus on Cotton Thread. IEEE Sens. J. 2018, 18, 4358–4363.

[13] Catalán-Gómez, S.; Briones, M.; Cortijo-Campos, S.; García-Mendiola, T.; de Andrés, A.; Garg, S.; Kung, P.; Lorenzo, E.; Pau, J.L.; Redondo-Cubero, A. Breast Cancer Biomarker Detection through the Photoluminescence of Epitaxial Monolayer MoS2 Flakes. Sci. Rep. 2020, 10, 16039.

[14] Hummers, W. S.; Offeman, R. E. (1958). "Preparation of Graphitic Oxide". Journal of the American Chemical Society. 80 (6): 1339.

[15] Sadri, Rad (2017). "Experimental study on thermo-physical and rheological properties of stable and green reduced graphene oxide nanofluids: Hydrothermal assisted technique". Journal of Dispersion Science and Technology. 38 (9): 1302–1310.

[16] S. Ghosh, I. Calizo, D. Teweldebrhan et al., "Extremely high thermal conductivity of graphene: prospects for thermal management applications in nanoelectronic circuits,"Applied Physics Letters, vol. 92, no. 15, p. 151911, 2008.

[17] Z.-S. Wu, W. Ren, L. Gao et al., "Synthesis of graphene sheets with high electrical conductivity and good thermal stability by hydrogen arc discharge exfoliation," ACS Nano, vol. 3, no. 2, pp. 411–417, 2009.

[18] M. A. Rafiee, J. Rafiee, I. Srivastava et al., "Fracture and fatigue in graphene

nanocomposites," Small, vol. 6, no. 2, pp. 179–183, 2010.

[19] R. R. Nair, P. Blake, A. N. Grigorenko et al., "Fine structure constant defines visual transparency of graphene," Science, vol. 320, no. 5881, p. 1308, 2008.

[20] D. Cohen-Tanugi and J. C. Grossman, "Water desalination across nanoporous graphene," Nano Letters, vol. 12, no. 7, pp. 3602–3608, 2012.

[21] F. Schwierz, "Graphene transistors," Nature Nanotechnology, vol. 5, no. 7, pp. 487–496, 2010.

[22] Y.-K. Kim and D.-H. Min, "Preparation of the hybrid film of poly(allylamine hydrochloride)-functionalized graphene oxide and gold nanoparticle and its application for laserinduced desorption/ionization of small molecules," Langmuir, vol. 28, pp. 4453–4458, 2012.

[23] B. D. Cullity, Elements of X-ray Diffraction. Addison-Wesley Publishing, 1956.

[24] G. Ali Al-Dahash, Q. Mohammed Salman, and M. F Haddawi, "Study the Effect of Copper (Cu) Doping on the Structure Properties of Zinc Oxide (ZnO) Prepared by Using Pulsed Laser Deposition (PLD)," J. kerbala Univ., vol. 13, no. 2, pp. 87–95, 2017.

[25] G. K. Williamson and R. E. Smallman, "III. Dislocation densities in some annealed and cold-worked metals from measurements on the X-ray debye-scherrer spectrum," Philos. Mag., vol. 1, no. 1, pp. 34–46, 1956.

[26]. A. M. Ramli, M. Z. Razali, and N. A. Ludin, Malaysian J. Anal. Sci., 21, 4, (2017)

[27] M. D. R. & K. A. A. G. H.Mohamed, S. N. Mazhir, ―The Influence of Bi content on The Structural and Optical Properties of thin TiO2 (1-x): Bix Films Prepared by pulse laser deposition, ‖ Int. J. Eng. Trends Technol., vol. 23, 2015.

[28] H. Kim et al., "Transparent conducting aluminum-doped zinc oxide thin films for organic light-emitting devices," Appl. Phys. Lett., vol. 76, no. 3, pp. 259–261, 2000.

[29] S. S. Chiad, K. H. Abass, T. H. Mubarak, N. F. Habubi, M. K. Mohammed, and A. A. Khadayeir, "Fabrication and study the structure, optical and dispersion parameters of PMMA with InCl3 additive," J. Glob. Pharma Technol., vol. 11, no. 4, pp. 369–374, 2019.

[30] M. G. Hutchins, O. Abu-Alkhair, M. M. El-Nahass, and K. Abd El-Hady, "Structural and optical characterisation of thermally evaporated tungsten trioxide (WO3) thin films," Mater. Chem. Phys., vol. 98, no. 2–3, pp. 401–405, 2006.

[31] S. J. Mousavi, ― First ‐ Principle Calculation of the Electronic and Optical Properties of Nanolayered ZnO Polymorphs by PBE and mBJ Density Functionals, ‖ J. Optoelectron. Nanostructures, vol. 2, no. 4, pp. 1 ‐ 18, 2017.

[32] M. Thakurdesai, N. Kulkarni, B. Chalke, and A. Mahadkar, "SYNTHESIS OF CdSe FILMS BY ANNEALING OF Cd/Se BILAYER," Chalcogenide Lett., vol. 8, no. 3, pp. 223–229, 2011.

[33] S. Sönmezoğlu, A. Arslan, T. Serin, and N. Serin, "The effects of film thickness on the optical properties of TiO2–SnO2 compound thin films," Phys. Scr., vol. 84, no. 6, p. 65602, 2011.

[34] G. Aytaç, "Effect of Au Nanoparticles Doping on The Properties of TiO2 Thin Films", Materials Science (Medžiagotyra), (2014), vol. 20, no.1, p. 1392–1320.

[35] D. Na, L. Satyanarayana, G.-P. Choi, Y.-J. Shin, and J. S. Park, "Surface morphology and sensing property of NiO-WO3 thin films prepared by thermal evaporation," Sensors, vol. 5, no. 12, pp. 519–528, 2005.